S24-29

Fundamental Studies of Solidification in Microgravity Using Real-Time X-Ray Microscopy

039094

Principal Investigator: Dr. Peter A. Curreri; NASA Marshall Space Flight Center (MSFC)
Co-Principal Investigator: Dr. William Kaukler; University of Alabama, Huntsville
Co-Investigators: Dr. Subhayu Sen; Universities Space Research Association
Dr. Biliyar N. Bhat; NASA Marshall Space Flight Center

Introduction

This research applies a state of the art X-ray Transmission Microscope, XTM, to image (with resolutions up to 3 micrometers) the solidification of metallic or semiconductor alloys in real-time. We have successfully imaged in real-time: interfacial morphologies, phase growth, coalescence, incorporation of phases into the growing interface, and the solute boundary layer in the liquid at the solid-liquid interface [1-9]. We have also measured true local growth rates and can evaluate segregation structures in the solid; a form of in-situ metallography. During this study, the growth of secondary phase fibers and lamellae from eutectic and monotectic alloys have been imaged during solidification, in real-time, for the first time in bulk metal alloys.

Current high resolution X-ray sources and high contrast X-ray detectors have advanced to allow systematic study of solidification dynamics and the resulting microstructure. We have employed a state-of-the-art sub-micron source with acceleration voltages of 10-100 kV to image solidification of metals. One useful strength of the XTM stems from the manner an image is formed. The radiographic image is a shadow formed by x-ray photons that are not absorbed as they pass through the specimen. Composition gradients within the specimen cause variations in absorption of the flux such that the final image represents a spatial integral of composition (or thickness).

The ability to image these features in real-time enables more fundamental and detailed understanding of solidification dynamics than has previously been possible. Hence, application of this technique towards microgravity experiments will allow rigorous testing of critical solidification models.

XTM Results:

The XTM has been applied to obtain information fundamental to solidification of metallic systems. (Refer to ref. [2,6,8] for a good description of the technique.) A diverse array of alloys have been studied with the XTM:

1. The solid-liquid planar interface of *pure* aluminum was studied with and without second phase insoluble particles (spherical voids, cylindrical holes, and zirconia spheres).
2. Single-phase alloys of Al with Cu, Ag, Au, and Mg were examined to observe solutal distribution effects at the interface, interface instabilities from planar to cellular, or interactions with the interface shape due to the thermal field perturbations caused by insoluble second phase particles both at equilibrium and during solidification. One major aspect of this was the study of particle pushing in support of the PEP flight experiment. The dynamics of solid/liquid interface shape evolution near an insoluble particle showed the limits to the applicability of some analytical models.
3. Two-phased eutectic alloys of Al with $CuAl_2$ or $AuAl_2$ were studied to observe lamellar and fibrous growth morphologies respectively.
4. Two-phased monotectic alloys of Al with In, Bi, or Pb were studied to observe growth morphologies and solute distributions. Fibers were observed to form in Al-Pb and Al-Bi.
5. Al-Mn-Si alloys were examined for nucleation and growth of precipitates in the melt.
6. Planar interfaces in pure Zn were observed to demonstrate that other base materials than Al could be used.

Solid-Liquid Interface in the Vicinity of an Insoluble Particle in the Melt

The distribution of insoluble particles in a metal casting depends primarily on the interaction of the particles with the solid/liquid (s/l) interface during the solidification process. This is true whether the particles are solid, liquid or gaseous. It has been experimentally demonstrated that there exists a critical interface

velocity, V_{cr} at which the transition from particle pushing to engulfment occurs and V_{cr} decreases as particle radius increases, following a power law.

It has been postulated that the thermal conductivity ratio, μ between the particle and the liquid matrix affects the transition from particle pushing to engulfment. When $\mu<1$ the particle acts as a heat sink and this results in a lower temperature and faster growth velocity of the interface just below the particle. Subsequently a convex protuberance or a bump is formed on the solidification front behind the particle. For systems with $\mu>1$ the particle acts as a source of heat and this lowers the growth velocity of the interface behind the particle. This results in a trough formation or a concave depression below the particle. Finally, when $\mu=1$ the thermal field is unperturbed and consequently, the interface remains planar. Neglecting forces due to convective flow and gravitational acceleration, the two main forces acting on a particle suspended in liquid metal are due to drag and interfacial energies. The (attractive) drag force between the particle and the s/l interface is expressed as:

$$F_D = 6\pi\eta V \frac{R^2}{d}\mu^2 \qquad 1$$

where F_D= drag force, h = viscosity, V= interface velocity, R = particle radius and d = distance between the interface and the particle. Equation 1 accounts for the contribution of localized deviations from planarity when the interface approaches the particle. The (repulsive) interfacial force is expressed as :

$$F_I = 2\pi R\Delta\sigma_o\left(\frac{a_o}{a_o + d}\right)^2 \mu \qquad 2$$

where, F_I = interfacial force, $\Delta\sigma_0$ = difference in interfacial energies between particle/liquid and particle/solid and a_0 = interatomic distance. Equations 1 and 2 show that the force field acting on the particle is influenced by the localized deviation of the s/l interface in the proximity of the particle. Furthermore, the localized deviation will also effect the critical velocity for engulfment. Hence, the objective of this investigation was to experimentally quantify the nature and extent of this deviation as a function of μ, particle radius, R , and the distance between the particle and the interface, d.

Figure 1 illustrates the effect of a 500 μm diameter ZrO_2 particle on a stationary and a growing interface [1]. When the stationary interface has almost made contact with the particle, that is d≈8 μm (Figure 1a), a convex perturbation or a bump formation on the interface is noticed. The behavior of a growing s/l interface interacting with 500 μm diameter ZrO_2 particle is, however, different compared to a stationary interface. With a translation velocity of 3 μm/s, a distinct depression or trough formation was noticed on the tip of the original convex protuberance (Figure 1b), at a distance of d=40 μm. Whereas, for a stationary interface interacting with the particle no such trough was detected.

The two dimensional analytical solution (in spherical co-ordinates) which describes the shape of an interface near a particle has several simplifying assumptions. For example, it neglects the effect of latent heat of fusion of the matrix and the particle heat capacity. Further, the thermal conductivities of the liquid and solid matrix are assumed to be equal. Consequently, the effect of these parameters is not accounted for by this analytical model. After applying appropriate boundary conditions, the isotherm for the melting point of the interface is described as:

$$Cos\theta = \frac{(R+d)\left[1+\frac{a}{b}\right]}{r\left[1+a\left(\frac{R}{r}\right)^3\right]} \qquad 3$$

where, $a = \frac{1-\mu}{2+\mu}$ and $b = \left(1+\frac{d}{R}\right)^3$.

By definition, the interfacial radius of curvature, R_I, below the particle can be expressed as:

$$R_I = \frac{2a-b}{3a}(R+d) \qquad 4$$

Here, only the analytical solution for interface shape prediction is compared to the experimental results. Fig. 2(a) shows the experimental results and the analytical solution for a pure Al stationary interface at a distance of 8 μm from a 500 μm diameter spherical ZrO_2 particle. Since the thermal conductivity of ZrO_2 is less than liquid Al, a protuberance is expected at this separation. Indeed, the analytical model is in agreement with the experimental measurements. Fig. 2(b) is a comparison of the shape of the growing interface with that predicted by the analytical model. The analytical model predicts a convex protuberance for these conditions, in contradiction with the experimental observations. In the absence of latent heat effects, the predictions of the analytical model are consistent with the experimental results for equilibrated interfaces. However, the analytical model fails in the case of a moving interface probably due to the continuous evolution of latent heat. Based on the above analysis it can be stated that the initial stages of interaction between a particle and an interface is not a steady state process. There appears to be a constant adjustment of the equilibrium distance between the particle and the interface as dictated by the thermal field and the force field (attractive and repulsive). The thermal field is not only dictated by the thermal conductivity ratio but also the latent heat entrapment between the particle and the interface during solidification.

Eutectic and Monotectic Second Phase Structures

The application of XTM for the study of solidification fundamentals was *initially* limited to a resolution of 25 μm for real-time imaging. The study of the dynamics of formation of secondary eutectic and monotectic droplets and fibers required a resolution on the order of 5 μm. Our recent advances in XTM furnace design have increased the real-time magnification (during solidification) for the XTM from 40X to160X. The increased magnification has enabled for the first time XTM imaging of real-time growth of fibers and particles with diameters of 3-8 μm and of eutectic lamellae with 12 μm spacing. Figure 4 and 3a, illustrate these respectively. To ensure the lamellar features observed were not artifacts, the lamellar spacings were measured during growth and after growth by sectioning and conventional metallography. All the spacings measured were consistent with themselves and with previously published measurements; Figure 3b.

At low growth rates (2 μm/sec) rejection of solute into the liquid by the solid was frequently observed using XTM in the Pb and In based Al monotectic alloys. The solute boundary layer was also observed in Bi monotectic specimens but unlike the In and Pb monotectics, was found to be clear of precipitated droplets. Generally, the solute layer was observed to extend 75 to 100 μm from the solid into the melt at the s/l interface for the growth rates used.

We have studied the kinetics of formation and morphological evolution of secondary fibers and particles in Al-Bi monotectic alloys. We observed a previously unreported velocity dependent thermo-capillary depletion mechanism for Bi-rich liquid which can penetrate many fiber diameters. At a reduced velocity approaching zero, the secondary liquid (L2) rods intersecting the interface began to 'drain' or exude from their cylindrical cavity and form droplets at the solid-liquid interface that grew to about 22 μm diameter. They detached and moved quickly up the thermal gradient. Within about 3 minutes the Bi-rich L2 rods were depleted to a distance of about 50 μm into the solid. This is illustrated in Figure 4a. Some Bi-rich droplets were seen to migrate up the gradient *during* solidification as well. Contrast this to the formation of droplets within the solute layer in the melt of the Al-Pb and Al-In monotectics. These droplets stayed where they formed only to be engulfed by the matrix. One hypothesis is that the alternate behaviors stem from interfacial energy differences between the three systems. We feel from the rate of depletion effects, and the observed migration of the droplets during solidification, that the phenomenon be considered in solidification kinetic models for monotectics.

Figure 4b shows the real-time image resulting from a translation rate increase from zero to 5 μm/sec. This image was taken following the 'depletion' scenario described above. The depleted zone behind the interface is visible in this radiomicrograph. The solidification transient developed a band of solid aluminum with very little bismuth. Only in a few places can some fibers or droplets be seen to form until composite growth is established as seen on the left side of this image. The solute had to build-up to a sufficient degree for the formation of the second phase precipitates. At the 5 μm/sec translation rate, it required about 100-200 μm of growth to permit the formation of the fully developed composite interface structure.

As far as we know, we have made the first real-time observations of bulk solidification morphology for Al-7.4 weight % Au on-eutectic alloy. Examples are shown in Figure 6. We observed this alloy with 5 μm resolution forming Al_2Au fibers (Figure 6a) or plates (Figure 6b, depending on growth rate) in an Al matrix. Additionally, the intermetallic fibers in this system were found to grow in advance of the s-l interface for growth rates above the fiber-plate transition velocity of ~1 μm/sec (Figure 6b). The extended Al_2Au phase fibers survived in the melt after translation was set to zero velocity for approximately 2 minutes. We noted thickening (ripening) of these Al_2Au phase fibers at this time. Some ripened fibers were about 25 μm thick and extended about 100 μm into the melt. It was observed over time (several minutes), that the coarsened, extended portions of the intermetallic phase eventually loosened from the matrix and settled to the bottom of the crucible. The existence of such a process and subsequently its kinetics would be nearly impossible to study with conventional solidification and quench techniques. We are not aware that this phenomena has been previously reported.

Solute Distribution in the Melt

Recently, the work focused on the quantification of the solute distribution in the melt in the vicinity of the s-l interface. A gas-quench apparatus was installed into the XTM furnace to permit post-solidification composition analysis. Very dilute (0.34 and 0.84 weight %) Al-Au alloys were solidified around the planar-cellular transition and gas-quenched. Quench rates were not sufficiently high (to date) to prevent cellular or dendritic breakdown of the interface. The resulting microsegregation made high-resolution solute profiling impossible. Fortunately, the solute boundary layer extends up to 2000 μm or more depending on growth rate so the solute concentration variation could be measured with lower resolution. Solute profiles were measured from low magnification film radiographs of the specimens grown at various rates. The quenched interface profile was measured as an intensity average across a 1 mm wide strip of the sample for 4 mm. One example growth rate will be shown here and compared to a model.

This measured profile was used to create a two-dimensional synthetic radiograph image such that the shade of gray used depended on the intensity value at each point along the profile. Using image processing techniques, this image was reduced in contrast (mathematically the profile amplitude was linearly reduced) until the gray level of the solid side of the interface matched the gray level of the specimen radiograph. This produced an image that matched the original in appearance. Each step required a different computer program because some steps require operator interaction and because a similar approach was taken to create a synthetic radiograph image from a model.

Using the Tiller, Rutter et al. model for interface diffusion and phase diagram data, a solute concentration curve was determined for Al-0.8Au growing at 5 μm/sec with the solute diffusion coefficient of 3 x 10^5 cm^2/sec.

These images were assembled into a single composite graphic shown in Fig. 5 a. Instead, the comparison needs to be made from graphs of these intensities or compositions. Figure 5b shows how well the images above match graphically. This figure superimposes the normalized gray level plots of the measured profile with the modeled profile for direct comparison. For profile measurements made on other specimens (not shown here), the solute distribution (concentration variation into the melt) in the quenched melt is nearly linear at the interface. The concentration profiles do not have the classic exponential rise to the interface. The model comes quite close with its diffusion limited profile shape and depth.

Acknowledgments

Thanks are extended to Pat Salvia in the foundry at Materials & Processes Lab. for casting the alloys and having the chemical analysis performed. We wish to thank NASA's Microgravity Science Division NRA Program for funding this work.

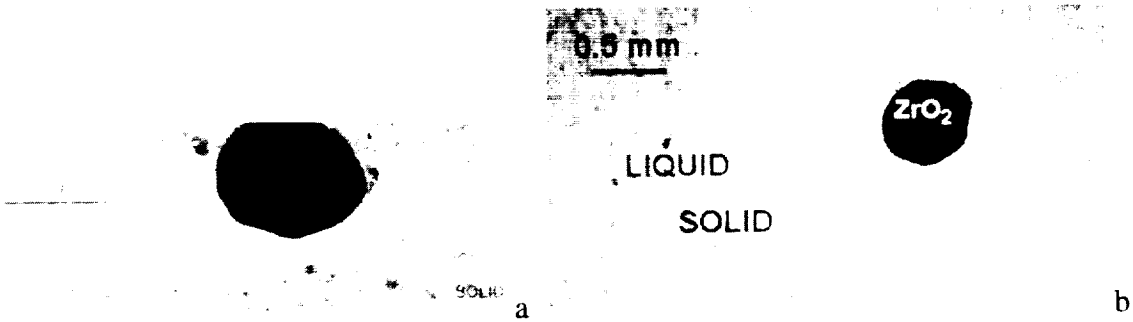

Fig. 1. (a) A x-ray radiograph of a planar s/l Al interface interacting with 500 μm diameter ZrO_2 particle at a distance of d=8 μm and (b) a video image of a transient s/l Al interface at a distance of d=40 μm from the ZrO_2 particle.

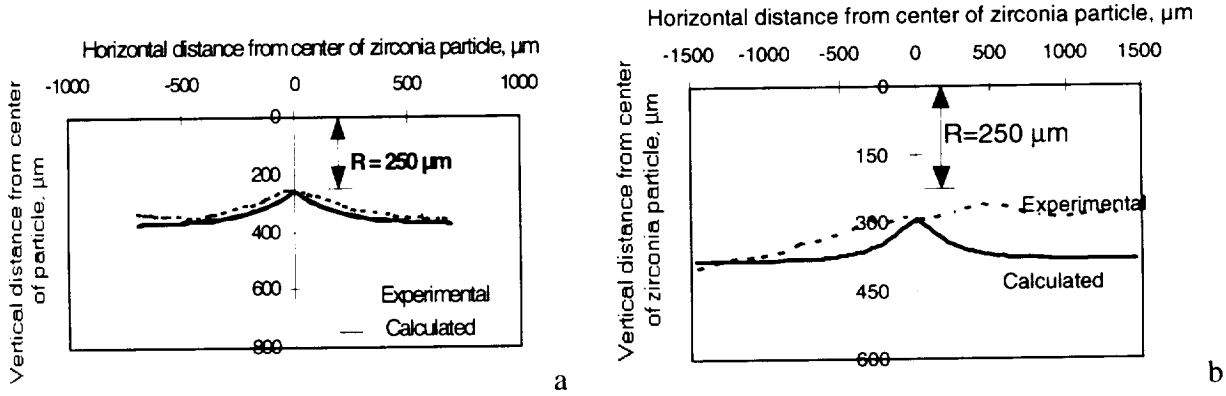

Fig. 2. Experimental results and analytical solutions for (a) a stationary s/l Al interface interacting with a 500 μm diameter ZrO_2 particle. The interface is at a distance of d=8 μm from the particle and (b) a moving s/l Al interface interacting with a 500 μm diameter ZrO_2 particle. The interface is at a distance of d=40 μm from the particle.

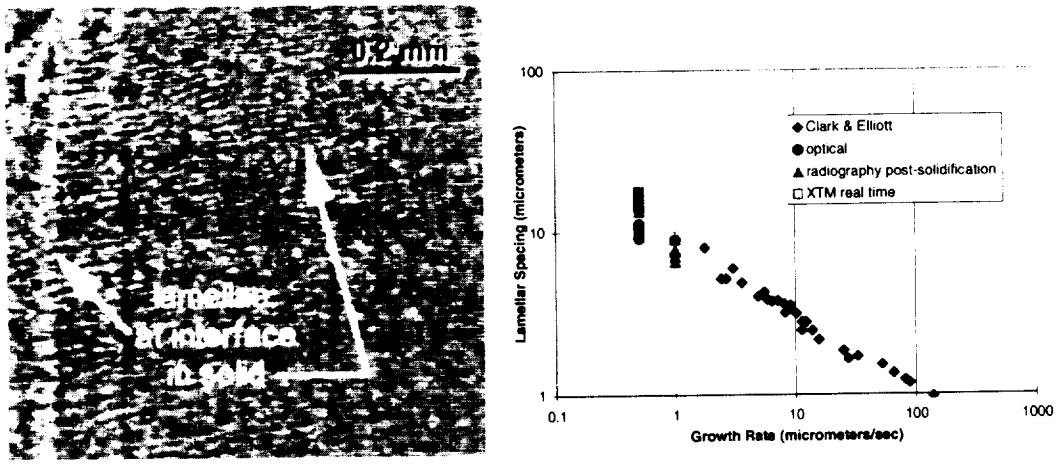

Figure 3 a and b. A) Digitally enhanced image showing lamellar morphology forming at solid-liquid interface. Translation rate 0.5 μm /sec, gradient 4160 K/m, $\lambda \approx 15$ μm. L is liquid. The lamellae are growing at a slight angle to the interface isotherm. B) Measured lamellar spacings compared to literature values. Optical and radiographic measurements coincide and all are consistent with Clark & Elliott.

Fig. 4 a,b. Real-time XTM images of Al-3.4 Bi monotectic. a) The translation at 3 μm/sec was halted for a few minutes and some of the liquid-2 fibers at the interface ejected themselves leaving a whiter region behind (arrows). Note also the 3D particle array on the right. b) Captured during the resumption of the growth, now at 5 μm/sec translation rate. Here, a band of solid with lower Bi concentration [A] is seen adjacent to the previously halted interface with some sporadic liquid-2 fibers and droplets forming within this transition [B]. The solid-liquid interface has returned to a composite structure [C].

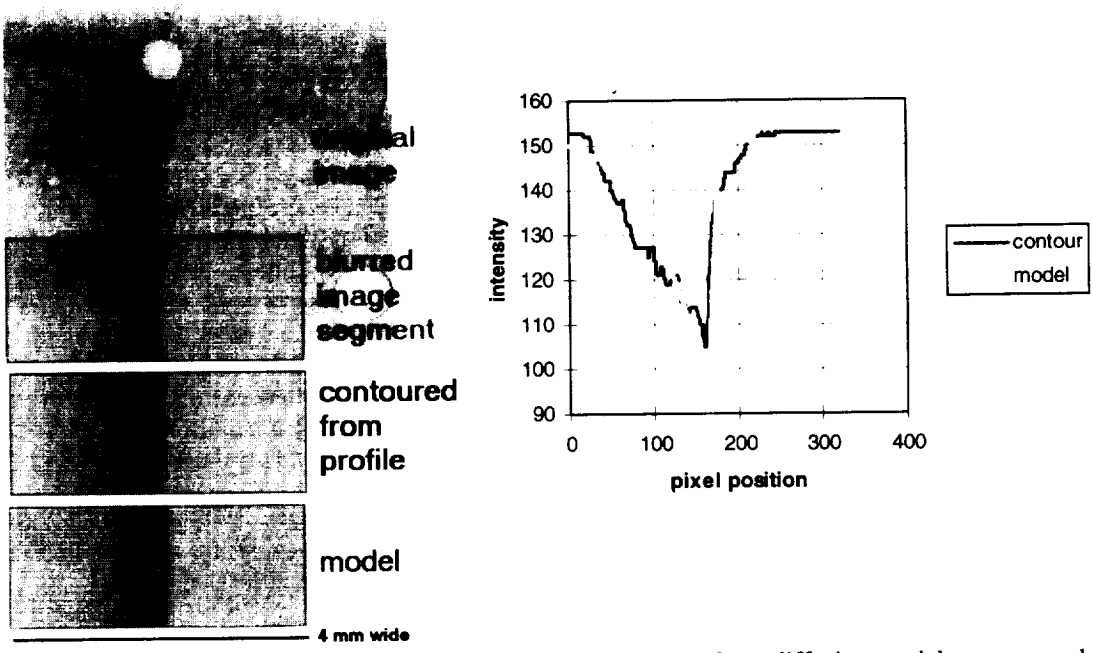

Figure 5 a and b. Results from comparison of synthetic radiographs from diffusion model to measured solute concentration induced intensities. a) Top shows post-quench radiograph of Al-0.8 Au grown at 5 μm/sec. Melt is on the left of interface. Next, is a segment smoothed by unidirectional blurring and then below that the synthetic radiograph made from a 2-D contour plot of the measured intensity profile from a 1 mm wide band in the radiograph. The bottom image was constructed from a diffusion model for the same solidification conditions and selective x-ray absorption by the constituents for the x-ray spectrum applied. b) The gray level intensities from the bottom 2 images in a) are superposed to show the reasonable fit between the model and the radiograph. Note how the measured composition contour has a linear form in the melt.

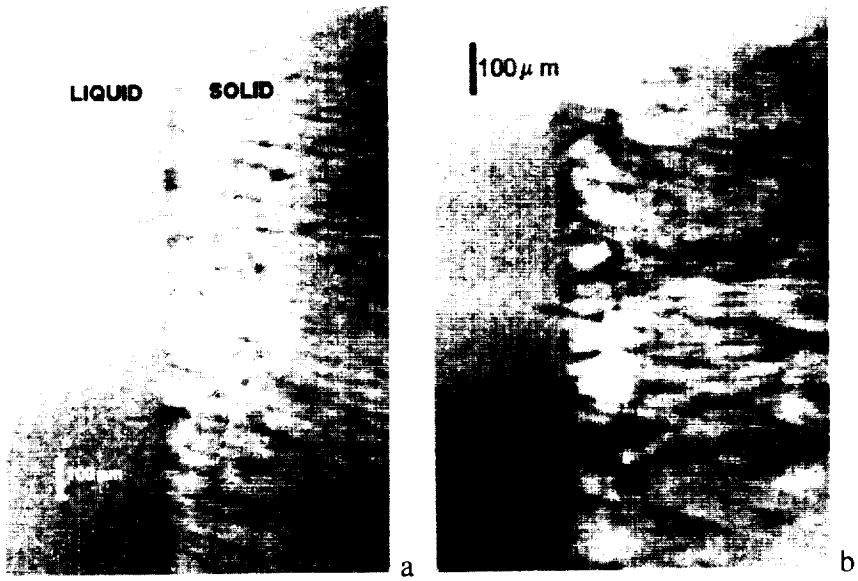

Figure 6 a (left, rate of about 2 μm/sec) and b (right, rate of about 1 μm/sec). Radiomicrographs of Al-Au eutectic during solidification. The microstructure is fibrous $AuAl_2$ in an Al matrix in a. b shows the degeneration of the fibers into plate-like features. The growth direction is to the left in a thermal gradient of 52 K/cm .

References

1. S. Sen, W. F. Kaukler, P. Curreri and D. M. Stefanescu (1997)"Dynamics of Solid/Liquid Interface Shape Evolution near an Insoluble Particle - An X-ray Transmission Microscopy Investigation",: Metallurgical and Materials Transactions A, 28A, pp. 2129-2135.
2. Kaukler, W. F. and P. A. Curreri (1996) "Advancement of X-ray Microscopy Technology and it's Application to Metal Solidification Studies," presented at the 1996 SPIE Technical Conference in Space Processing of Materials, Aug. 4, 1996, Ed. N. Ramachandran, 2809:34-44.
3. Curreri, P. A., Kaukler, W. F., Sen, S. and Peters, P. "Application of real-time X-ray Transmission Microscopy to Fundamental Studies of Metal Alloy Solidification", Spacebound 97 Proceedings, Canadian Space Agency; joint meeting with 9th International Symposium on Experimental Methods for Microgravity Materials Science, May 11-15 1997, Montreal Canada:72-84.
4. Curreri, P.A. and W. Kaukler (1996) "X-Ray Transmission Microscopy Study of the Dynamics of Solid/Liquid Interfacial Breakdown During Metal Alloy Solidification," Presented at 8th International Symposium on Experimental Methods for Microgravity Materials Science, Feb 4-8, 1996, Anaheim, CA, 125 TMS Annual Meeting, available on CD from TMS.
5. Kaukler, W. F. and P.A. Curreri, (1996) "X-Ray Transmission Microscopy of Al-Pb Monotectic Alloys During Directional Solidification," Presented at 8th International Symposium on Experimental Methods for Microgravity Materials Science, Feb 4-8, 1996, Anaheim, CA, 125 TMS Annual Meeting, available on CD from TMS.
6. Kaukler, W., F. Rosenberger, and P. A. Curreri (1997) "In-situ Studies of Precipitate Formation in Al-Pb Monotectic Solidification by X-ray Transmission Microscopy," Metallurgical Transactions, 28A:1705-1710.
7. Curreri, P. A., Kaukler, W. F. and Sen, S. "Real-time X-ray Transmission Microscopy for Fundamental Studies of Solidification: Al-Al_2Au Eutectic", CP420 Space technology and Applications International Forum-1998, The American Institute of Physics, 389-396.
8. Curreri, P.A. and W. F. Kaukler (1996) "Real-Time X-Ray Transmission Microscopy of Solidifying Al-In Alloys," Metallurgical Transactions 27A (3):801-808.
9. Curreri, P.A. and W. F. Kaukler (1995) "Real-Time X-Ray Transmission Microscopy of Solidifying Al-In Alloys," presented at The Metallurgical and Materials Society Annual Meeting, Las Vegas, NV, Feb. 12-16, 1995) published in Proceedings of 7th International Symposium on Experimental Methods for Microgravity Materials Science, Robert Schiffman, Ed., The Minerals, Metals and Materials Society, 93-101.